Chinese Chemical Letters 33 (2022) 5142–5146

Contents lists available at ScienceDirect

Chinese Chemical Letters

journal homepage: www.elsevier.com/locate/cclet

Chiral structures of 6,12-dibromochrysene on Au(111) and Cu(111) surfaces

Shijie Sun[a,1], Baijin Li[a,1], Boyu Fu[a], Zilin Ruan[a], Hui Zhang[a], Wei Xiong[a], Yong Zhang[a], Gefei Niu[a], Jianchen Lu[a], Xiaoqing Zuo[a], Lei Gao[b,*], Jinming Cai[a,*]

[a] Faculty of Materials Science and Engineering, Kunming University of Science and Technology, Kunming 650000, China
[b] Faculty of Science, Kunming University of Science and Technology, Kunming 650000, China

ARTICLE INFO

Article history:
Received 10 November 2021
Revised 10 December 2021
Accepted 29 December 2021
Available online 4 January 2022

Keywords:
Scanning tunneling microscope
Scanning tunneling spectroscopy
Non-contact atomic force microscope
Surface chirality
Chiral transition

ABSTRACT

Nanoscale low-dimensional chiral architectures are increasingly receiving scientific interest, because of their potential applications in many fields such as chiral recognition, separation and transformation. Using 6,12-dibromochrysene (DBCh), we successfully constructed and characterized the large-area two-dimensional chiral networks on Au(111) and one-dimensional metal-liganded chiral chains on Cu(111) respectively. The reasons and processes of chiral transformation of chiral networks on Au(111) were analyzed. We used scanning tunneling spectroscopy (STS) to analyze the electronic state information of this chiral structure. This work combines scanning tunneling microscopy (STM) with non-contact atomic force microscopy (nc-AFM) techniques to achieve ultra-high-resolution characterization of chiral structures on low-dimensional surfaces, which may be applied to the bond analysis of functional nanofilms. Density functional theory (DFT) was used to simulate the adsorption behavior of the molecular and energy analysis in order to verify the experimental results.

Low-dimensional supramolecular architectures constitute a significant section due to their fascinating new demonstrative applications in the fields of nanoscience and nanotechnology [1–3]. The bottom-up approach to the atomically precise syntheses of two-dimensional (2D) materials has become a regular fabrication method based on molecular self-assembly [4–9], Ullmann reaction [10], Bergman cyclization [11] and Glaser reaction [12] are also powerful means to construct organic materials. Fine organization of chiral behaviors [13–15] on solid surfaces has advanced over the years, yet still faces the need for the controlled and selective production of advanced chiral materials [16–18]. To date, the research of various chiral phenomena such as heteroatom-doped chiral graphene nanoribbons [19], chiral supramolecular bilayers [20] and on-surface synthesis hierarchical electronic structure [21] have become a new branch of nanoscience as well as begun to develop beyond the basic description. Real-space imaging at the single-molecule level is thus urgently required to understand the role of molecular chirality-related issues. Meanwhile, metal substrates with different catalytic properties have a great influence on the self-assembly of organic molecules on the surface [22,23]. Self-assembly of surface coordination arrangements presents a flexible way to distribute equally sized element centers evenly on a metal surface.

In this connection, probing low-dimensional architectures consisting of chiral or prochiral molecular select adsorbed at solid surfaces using scanning tunneling microscopy (STM) is considered as one of the most powerful and appropriate approaches to obtain an in-depth understanding of different chirality aspects at the molecule precise scale [24,25]. On metal surfaces, STM research has revealed the selective and rival adsorption behavior on 2D molecular self-assemblies, the constitution of superstructures in crystal engineering is extremely managed by directional forces and is susceptible to the effects of substrate properties and the extrinsic environment. Besides plenty of reports in the literature as regards the structural transformation of super networks by tuning precursors [26], external electric field [27], which is caused by the deposition time and physicochemical catalysis with the metal substrate is still rarely discussed. Whilst self-assembled nanostructures were transformed into final products with differentiation because multiple reaction pathways might simultaneously occur.

Herein, we report on the use of enantiomerically enriched molecular building blocks to demonstrate the performance of their intrinsic chirality along a sequence of different substrates. To demonstrate the influence of the select adsorption on the solid

* Corresponding authors.
E-mail addresses: lgao@kust.edu.cn (L. Gao), j.cai@kust.edu.cn (J. Cai).
[1] These authors contributed equally to this work.

https://doi.org/10.1016/j.cclet.2021.12.082
1001-8417/

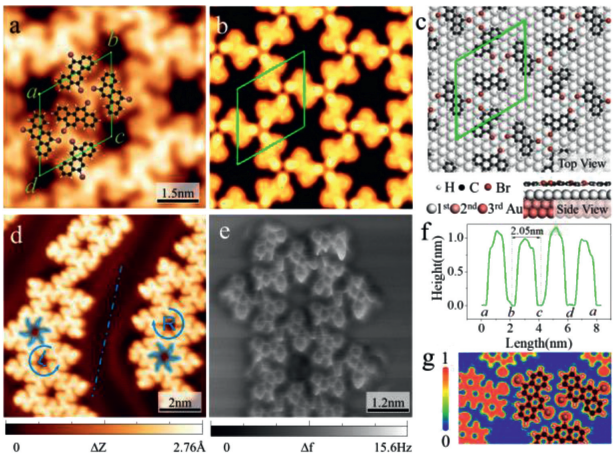

Fig. 1. Analysis of chiral pore structure on Au(111). (a) STM image of DBCh molecule self-assembled structure on Au(111), DBCh molecular structure model overlaid on the high-resolution STM image. The green rhombus indicates the unit cell of chiral networks. (b) DFT simulated STM image and (c) DFT-optimized adsorption configurations correspond to (a). (d) STM image contains two chiral domains of the networks. (The blue dotted line indicates the mirror symmetry axis of the chiral hole. The blue hexagram mark the chiral hole structures of L-chiral and R-chiral). (e) High-resolution nc-AFM image after CO-modified tip (U bias voltage, 2 mV; oscillation amplitude, 70 pm). (f) Lateral height image along with the green unit cell in (a), ab = ad = (20 ± 0.5) Å. (g) Theoretical calculated electron localization function of the DBCh networks.

substrates, 6,12-dibromochrysene (DBCh) was selected as the starting molecular building block, we have successfully fabricated two chiral supramolecular structures on Au(111) and Cu(111) substrates through molecular beam epitaxy (MBE) method. The apparent chirality structures were observed in atomic-resolution images as hexagonal hole lattice and chiral chains with different asymmetry depending on the adsorption position. As well, we have carried out density functional theory (DFT) based first-principles calculations for the molecular systems. DFT has played an essential role in understanding these materials by calculating the adsorption energy and simulated STM image can be directly compared with the experiment [28,29]. It has been revealed the significant influence of intermolecular halogen bonding and metal coordination on assembly behavior, which dominantly maintain the stability of diverse oligomers at low temperatures.

After the deposition of DBCh molecules on the Au(111) surface held at room temperature (RT), we observed a large-scale chiral regular types structure by STM under ultrahigh vacuum conditions (Fig. S1 in Supporting information), The self-assembled 2D molecular island is similar for both sub-monolayer about 0.7 monolayer coverage. In the high-resolution STM image (Fig. 1a), individual regular dart pores in the 2D porous molecular network are visible. The covered molecular model exhibits that the observed building units of the supramolecular hexagonal holes are molecular assemblies on their own. More interestingly, they contain exactly six molecules that are linked into a hexagonal supermolecule with a radius of 2 nm. To support the STM image-based structure distribution, an extensive structure search was performed by DFT to find the most stable structure, in addition to determining the number of DBCh molecules and the geometric coordinates of Br atoms. The calculated adsorption conformation agrees with the experiment, the Br atoms prefer to stabilize at triangle forming a self-assembled structure connected by halogen bonds. The simulated STM image (Fig. 1b) fully corroborates the experimental findings. Fig. 1c shows the DFT optimized models of DBCh molecules, the unit cell mark as the green parallelogram to show the periodicity of the self-assembled superstructure. The black, white and brown balls represent carbon, hydrogen and bromine atoms, respectively. The adsorption energy of this structure is $-4.277\,eV/nm^2$ by DFT energy analysis. According to the measurement results (Fig. 1f) from WSxM software [30], the unit cell parameters ab = ad = (20 ± 0.5) Å.

Supramolecular self-assembly of adsorbed molecules is the result of a competition between molecule substrate interactions and noncovalent intermolecular attractions arising from van der Waals forces, hydrogen bonds, and electrostatic interactions. Through meticulous observation and repeated sample preparation process, we found that this two-dimensional organic molecular pore structure has obvious surface chirality, which is caused by the optimization of the non-covalent bond structure between molecules. DBCh is chiral and planar as a result of inherent structure which causes a twisting of the central tetracene backbone around its axis and forces the two halogen atoms to rotate around their bonds. Although previous studies are interested in the self-assembly process of DBCh [24], their chirality research scale and real space characterization have not reached an ultra-high resolution. The inherent chirality of molecules gradually expands with the increase of the number of molecular beam epitaxies, a mirror-symmetric structure is formed on the surface of Au(111). To show the specific position of the chiral structure in Fig. 1d, we use counter-clockwise arrow to indicate left-handed (marked L) and clockwise arrow to indicate right-hand rotation (marked as R) respectively. The regular dart shape left on the symmetry axis (blue dotted line) has a counterclockwise arrangement of these lobes (L), while the one on the right follows a clockwise orientation (R), thus the domain of the molecule are mirror images of each other and reflect the chiral conformation of the molecule on the Au(111). The same chiral area distinguished by a blue dotted line in Fig. 1d as the axis of symmetry reveals the existence of surface chirality. Chiral structures show disjointed chains-rings which are constructed out of tiny building blocks. These structures are commensurate with the hexagonal periodicity of the Au(111) substrate but are sustained by the domain walls of the herringbone-reconstructed surface and at step edges. The theoretical commensurability of the constructions rules out site-specific bonding to the surface and indicates that the observed supramolecular assembly is restricted by intermolecular forces. As previously observed with numerous other aromatic adsorbates, also for chiral holes, the face-centered-cubic (fcc) region has a higher electron potential than the hexagonal-closed-packing (hcp) region, so is it favorable for adsorption on the former. The spontaneous self-assembly of single DBCh molecule results in the configuration of complex supramolecular structures. One of the three epitaxial equivalent orientations of each chiral hole is favored by maximizing its adsorption length on the fcc section, which will show more soliton intersections and hcp adsorption regions.

Therefore, it is necessary for single-molecule and halogen atomic resolution characterization and recognition. Through CO tip modification and qPlus sensor atomic force imaging technology, we obtained the bond resolution nc-AFM image, as shown in Fig. 1e, which reveals those structures with effective bonding angles of 60° are predominant on chiral dart holes. Fig. S2 (Supporting information) shows the high-resolution characterization of different regions to corroborate the molecular arrangement of the chiral structure. The fuzzy features observed in the nc-AFM image caused by the hydrogen atoms passivated the edge. Distortion of the benzene ring due to high repulsive forces between the tip and molecule. Theoretical simulations of the structural local work function in Fig. 1g reveal that no strongly interacting covalent bonds are formed between bromine atoms, but rather weakly interacting intermolecular halogen bonds. Interestingly, for brominated compounds, the halogen bond of Br-Br-Br dominates the self-assembly structure with triangular packing due to molecular charge distribution.

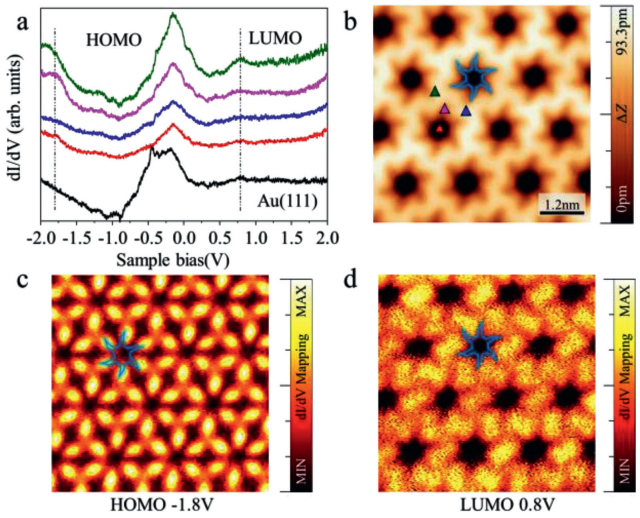

Fig. 2. Real-space electronic state detection. (a) Differential conductance (d*I*/d*V*) spectrum taken at the chiral porous structure marked by the different colored triangles in (b). The black curve represents the characteristic spectrum of the Au(111) surface. (b) STM topography image ($U = -0.25$ V, $I = 100$ pA) of chiral porous structure. (c) d*I*/d*V* mapping collected at energetic positions of states HOMO (Highest occupied molecular orbital) and (d) LUMO (Lowest unoccupied molecular orbital). Open feedback parameters for the d*I*/d*V* spectra: $U = -300$ mV, $I = 150$ pA. Tunneling parameters for the STM images and associated d*I*/d*V* maps: HOMO: $U = -1.8$ V, $I = 100$ pA; LUMO: $U = 0.8$ V, $I = 150$ pA.

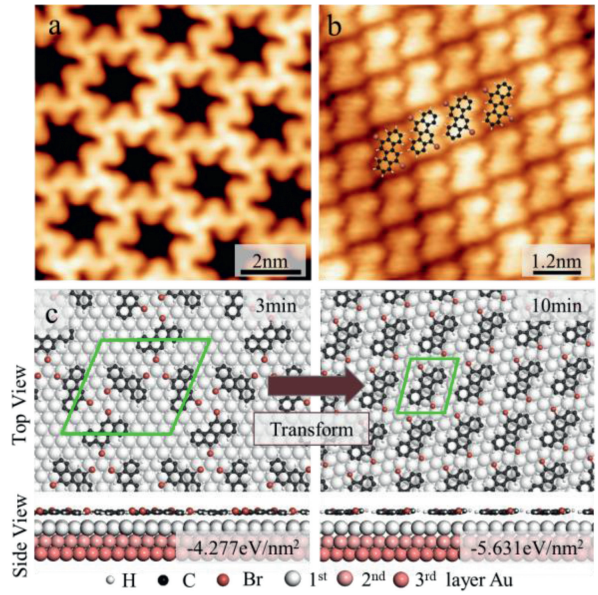

Fig. 3. Enantiomeric excess causes surface chiral transition. (a) STM image of submonolayer structure with deposition time of 3 min. $U = 1$ V, $I = 100$ pA. (b) DBCh molecular structure model overlaid on the STM image obtained by depositing DBCh molecules 10 min, $U = 0.5$ V, $I = 200$ pA. (c) Structural model diagram before and after chiral transformation. The lower inset identifies the structure adsorption energy.

In order to better understand the electronic state density information of the hole structure, we used density functional theory to combine real-space electronic detection to reveal that periodic lattice electrostatic landscape confines two-dimensional electron gas between molecular backbone lattice. Scanning tunneling spectroscopy characterizes this two-dimensional material result (Fig. 2), and shows that the highest electron occupied orbital (HOMO) and the lowest electron occupied orbital (LUMO) of the structure are 1.8 V and 0.8 V with obvious peaks on the d*I*/d*V* spectrum line (Fig. 2a) respectively. We observe the distinct peaks near the −0.45 V in Fig. 2a which are caused by the work function of Au surface. These peaks also appear frequently in the STS curves in the previous literature. The black curve has only characteristic peak revealing the absence of adsorbed impurities on the tungsten tip. Due to the obvious difference in the electron filling distribution between the periodic pores and the molecular backbone, the two-dimensional material structure is similar to a nano-sieve, which can be used to filter organic substances or desalinate seawater. It can also be used as an organic substrate to participate in the research of the two-dimensional structure of the host and guest.

Given that monomers and hexamer agglomerate into islands, the molecular environment (and thus the intermolecular interplays that could conceivably influence the racemization barriers) is expected to differ substantially for different molecular coverages. Due to the enantiomeric excess seems to be slightly amplification across subsequent stages, the changes remain beyond the structural carrying capacity, making this expansion nearly meaningful. Therefore, our results unambiguously confirm that the reactant chirality is transferred across the Au(111) substrate-supported reactions with the increasingly high arrangement denseness and longer evaporation time (Fig. 3). We controlled the deposition time to 10 min, the chiral pores disappeared, and a tightly packed full monolayer structure was obtained, as shown in Fig. 3b. This is due to the increase in the number of precursors, and the tightly packed have lower adsorption energy. The principle of thermodynamics promotes this chiral conversion. The concentration of molecule precursor controllable chirality transformation on the Au(111), there existed a single type of halogen bonding interactions between interplanar molecules. Through rationalizing the chiral transform mechanism at the molecular level, our findings are relevant for the recognition of cooperative supramolecular assembly in multiple-component systems. Fig. S3 (Supporting information) shows the typical herringbone reconstruction of Au(111) is visible through the molecular island faintly, the Au reconstruction is neither modified nor elevated upon adsorption of the molecules, meaning a weak molecule-substrate interaction. Actually, the manipulation principle of the assembled structure by all the DFT calculations is based on minimized energy regulation. Calculating the adsorption energy of this tightly packed configuration as -5.631 eV/nm^2, since the self-assembly systems prefer to low form energy close-packed patterns in a 2D layer, which are favored for enthalpy reasons [31].

As is clearly indicated from the STM measurements, the dehalogenation reaction of DBCh molecules deposited on a RT substrate has occurred due to the catalytic properties of the Cu substrate, which is consistent with the previous work [11,32]. Cu(111) was engaged as a substrate because its catalytic activity is generally considered to be higher than Au(111). Upon deposition of DBCh on Cu(111) held at RT, one-dimensional (1D) chiral polymers were observed, regardless of the molecular coverage (Fig. 4). We find that the stability of the structure benefits from the maximum number of hydrogen bonds and metal coordination bonds connected molecular backbone. The formation of this chain structure is due to the removal of halogens from the precursor molecules and the formation of metal coordination bonds between the molecular radicals and the copper substrate. It is apparent that the 1D polymer chains consist of two types of enantiomers linearly connected. The chiral symmetry property of the mirror image is marked with L and R respectively. In the high-resolution STM image in Fig. 4a, individual monomers within the 1D chiral polymer can be distinguished, the free Br atom between the chiral 1D chain was observed. The depth of the Br atom amounts to about 1.8 Å, which is equal to the height of a mono step of the precursor molecule (1.9 Å).

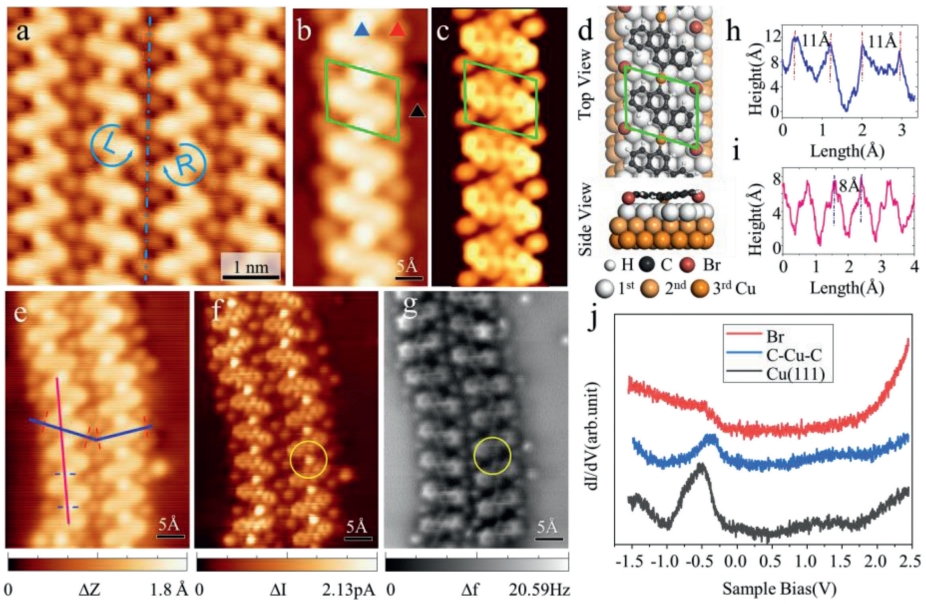

Fig. 4. Analysis of one-dimensional chiral chains on Cu(111). (a) The high-resolution STM image. The blue dotted line represents the mirror symmetry axis, the two sides are marked with L and R respectively as a left-handed and right-handed 1D polymer chain. (b) Single metal coordination chain and (c) correspond DFT simulated STM image. (d) Top and side views of 1D chain after structure-optimized. The green parallelogram represents the structural unit cell. (e) STM image of low coverage and nc-AFM analysis area. (f) The bond-resolved STM image in constant height mode after CO modification of the tip corresponds to (e). (g) An nc-AFM image (U bias voltage, 2 mV; oscillation amplitude, 70 pm) of the same area in (e). The yellow circle marks the position of the metal coordination bond C-Cu-C. (h, i) The line profiles along the blue line and the pink line in (e) show the single molecular length and molecular spacing of the 1D chiral chain, respectively. (j) Points d*I*/d*V* spectrum of the labeled triangle in (b).

For further energy analysis and structural simulation, we established the DFT model simulation with the green parallelogram in Fig. 4b as the unit cell to obtain the STM image as shown in Fig. 4c. The adsorption energy of the 1D chiral chain after structure optimization (Fig. 4d) is $-9.398\,eV/nm^2$. The experimentally measured distance between two monomers is found to be 0.8 ± 0.1 nm (Fig. 4i), which is in excellent agreement with the simulative determined monomer-to-monomer distance for the optimized geometry of the Cu-coordinated dimer (0.8 nm). The point STS spectrum curves obtained from probing the three triangular positions marked in Fig. 4b are shown in Fig. 4j. The peak intensity of the electronic eigenstate on the C-Cu-C metal coordination bond is weaker than that on the Cu(111) surface while the intensity of the peak on the bromine atom largely disappears. The metal coordination bond (yellow circle marked in Fig. 4f) is a bright spot in bond-resolved STM and a dark spot in nc-AFM image. It is due to the fact that metal atoms are located at a lower position and have a higher electronic density of states than small organic molecules. The simulated side view in Fig. 4d shows that the 1D chains are periodically twisted due to the Cu atoms of the ligand bonds being closer to the surface.

Therefore, it can be inferred that a 1D organometallic chiral polymer automatically forms on Cu(111) enabled through the debromination of DBCh at RT which is promoted by the comparably high catalytic activity of the Cu surface. In STM we observed the coexistence of both left- and right-handed polymers on Cu(111) in the same area. Analyzing the results gained for molecule assemble coupling of DBCh on Au(111) and Cu(111) we conclude that a chiral-selective configuration occurs for the 1D chiral polymers dependence of the substrate. An inherent judgment may be the establishment of different bonding motifs upon the on-surface coupling regression on Au(111) and Cu(111) (halogen bonds and C-Cu-C coordination bonds, respectively). For the case of the chiral 1D chiral polymers, the majority polymers align along within the $[1\bar{1}0]$ directions of the Cu(111) surface. Fig. S4 (Supporting information) shows the atomic resolution of the Cu(111) surface, marking the substrate orientation. For the chiral 1D polymer, the Cu adatoms order linearly and if a corresponding arrangement of the monomers is assumed the adatoms are then regularly adsorbed on the related lattice sites. In contrast, if achiral 1D organometallic polymers are formed, the Cu adatoms will describe a zigzag line and a commensurate organization of the adatoms will be no longer possible. Different adsorption sites of the adatoms for the achiral polymer could be slightingly less preferred and the chiral organometallic polymers would be favored consequently. Among others, the metal-organic coordination motifs, due to their specific coordination sizes, arrangements, and thermic stability, are much effective to manage the reaction pathway and the morphology of the resultant structures. Consideration of the registry between these films then allowed us to manage the chirality of the surface region, which is challenging with ensemble techniques that typically demand bulk single-crystal samples. As the architectural chirality sets the chirality of physical property in this family of materials, this capability is important in harnessing these novel chiral textures for future high-density storage applications.

In conclusion, we have successfully constructed large-scale, high-quality 2D self-assembled chiral networks on Au(111) and the 1D chiral chain on Cu(111) respectively. The two structures were characterized by ultrahigh atomic resolution. The configuration of the network is controlled by intermolecular halogen bonding. The molecule prefers the sites with the maximum number of halogen bonds, which serves to stabilize the network. The arrangement of chiral chains on the surface of Cu(111) is due to the formation of C-Cu-C bonds. The STS results of the chiral hole structure formed on the Au(111) surface show that the density of electronic states is different between the hole center and the molecular framework, which has obvious significance for the subsequent host-guest studies. This work provides a prototype for investigating on-surface chiral networks. Although there are still undoubted challenges in stereo imaging of chiral molecules, the above innovative studies through atomic-level imaging of surface chiral structures, including chirality transform in chiral molecule assemblies, have promoted revealing surface chirality.

Declaration of competing interest

The authors declare that they have no known competing financial interests or personal relationships that could have appeared to influence the work reported in this paper.

Acknowledgments

This work was supported by the National Natural Science Foundation of China (Nos. 51861020, 61901200 and 12064020), the National Recruitment Program for Young Professionals (No. 132310976002), the Yunnan Province Science and Technology Plan Project (No. 2019FD041), the Strategic Priority Research Program of Chinese Academy of Sciences (No. XDB30010000), the Reserve Talents for Yunnan Young and Middle Aged Academic and Technical Leaders (No. 2017HB010), the Yunnan Province for Recruiting High-Caliber Technological Talents (No. 1097816002). Yunnan Fundamental Research Projects (No. 202101AU070043).

Supplementary materials

Supplementary material associated with this article can be found, in the online version, at doi:10.1016/j.cclet.2021.12.082.

References

[1] J. Lu, D.L. Bao, H. Dong, et al., J. Phys. Chem. Lett. 8 (2017) 326–331.
[2] H. Song, H. Zhu, Z. Huang, et al., ACS Nano 13 (2019) 7202–7208.
[3] D. Wang, M. Yang, Arramel, et al., ACS Appl. Mater. Interfaces 12 (2020) 35547–35554.
[4] J. Cai, P. Ruffieux, R. Jaafar, et al., Nature 466 (2010) 470–473.
[5] C. Sánchez-Sánchez, J.I. Martínez, N.R. Arbol, et al., J. Am. Chem. Soc. 141 (2019) 3550–3557.
[6] Q. Xue, Y. Zhang, R. Li, et al., Chin. Chem. Lett. 30 (2019) 2355–2358.
[7] J. Hou, B. Tu, Q. Zeng, et al., Chin. Chem. Lett. 31 (2020) 353–356.
[8] R. Li, X. Zhang, N. Xue, et al., Acta Phys. Chim. Sin. 37 (2020) 2011060.
[9] Y. Wang, M. Zhong, J. Li, et al., Chin. Chem. Lett. 33 (2022) 1074–1076.
[10] E. Lewis, M. Marcinkowski, C. Murphy, et al., Chem. Commun. 53 (2017) 7816–7819.
[11] L. Li, S. Mahapatra, D. Liu, et al., ACS Nano 15 (2021) 3578–3585.
[12] P. Ou, X. Zhou, F. Meng, et al., Nanoscale 11 (2019) 13600–13611.
[13] H. Kong, Y. Qian, X. Liu, et al., Angew. Chem. 132 (2020) 188–192.
[14] T. Ueda, Y. Sera, H. Adachi, et al., Phys. Rev. B 103 (2021) 014506.
[15] C.K. Ma, Y. Wang, M.X. Shi, et al., J. Phys. Chem. C 125 (2021) 335–340.
[16] J. Tschakert, Q. Zhong, D. Martin-Jimenez, et al., Nat. Commun. 11 (2020) 5630.
[17] N. Merino-Díez, M.S. Mohammed, J. Castro-Esteban, et al., Chem. Sci. 11 (2020) 5441–5446.
[18] C. Kulkarni, A.K. Mondal, T.K. Das, et al., Adv. Mater. 32 (2020) 1904965.
[19] X.Y. Wang, J.I. Urgel, G.B. Barin, et al., J. Am. Chem. Soc. 140 (2018) 9104–9107.
[20] H. Cao, S. De Feyter, Nat. Commun. 9 (2018) 3416.
[21] C. Steiner, J. Gebhardt, M. Ammon, et al., Nat. Commun. 8 (2017) 14765.
[22] A. Ugolotti, S.S. Harivyasi, A. Baby, et al., J. Phys. Chem. C 121 (2017) 22797–22805.
[23] J. Ren, D.L. Bao, L. Dong, et al., J. Phys. Chem. C 121 (2017) 21650–21657.
[24] T.A. Pham, B.V. Tran, M.T. Nguyen, et al., Small 13 (2017) 1603675.
[25] S. Stolz, A.V. Yakutovich, J. Prinz, et al., Angew. Chem. 132 (2020) 18336–18340.
[26] J. Hu, K. Shen, J. Hu, et al., ChemPhysChem 20 (2019) 2376–2381.
[27] W. Li, S. Xu, X. Chen, et al., Chin. Chem. Lett. 32 (2021) 480–484.
[28] C. He, R. Sun, L. Fu, et al., Chin. Chem. Lett. 33 (2022) 527–532.
[29] J. Yu, C. He, C. Pu, et al., Chin. Chem. Lett. 32 (2021) 3149–3154.
[30] I. Horcas, R. Fernández, J. Gomez-Rodriguez, et al., Rev. Sci. Instrum. 78 (2007) 013705.
[31] J. Huan, X. Zhang, Q. Zeng, Phys. Chem. Chem. Phys. 21 (2019) 11537–11553.
[32] M. Telychko, J. Su, A. Gallardo, et al., Angew. Chem. 131 (2019) 18764–18770.